Reaction of the Hydroxyl Radical with Phenol in Water Up to Supercritical Conditions

ARTICLE *in* THE JOURNAL OF PHYSICAL CHEMISTRY A · APRIL 2007

Impact Factor: 2.69 · DOI: 10.1021/jp0665325 · Source: PubMed

Reaction of the Hydroxyl Radical with Phenol in Water Up to Supercritical Conditions

Julien Bonin, Ireneusz Janik, Dorota Janik, and David M. Bartels*

Radiation Laboratory, University of Notre Dame, Notre Dame, Indiana 46556

Received: October 4, 2006; In Final Form: January 9, 2007

The rate constants for the reactions of phenol with the hydroxyl radical ($OH^•$) in water have been measured from room temperature to 380 °C using electron pulse radiolysis and transient absorption spectroscopy. The reaction scheme designed to fit the data shows the importance of an equilibrium, giving back reactants ($OH^•$ radical and phenol) from the dihydroxycyclohexadienyl radical formed by their reaction, and the non-negligible contribution of the hydroxycyclohexadienyl radical absorption from $H^•$ atom addition. The accuracy of the reaction scheme and the reaction rate constants determined from it have been determined by the analysis of two different experiments, one under pure N_2O atmosphere and the second under a mixture a N_2O and O_2. We report reaction rates for the $H^•$ and $OH^•$ radical addition to phenol, the formation of phenoxyl, the second-order recombination, the reaction of dihydroxycyclohexadienyl with O_2, and the decay of the peroxyl adduct. Nearly all of the reaction rates deviate strongly from Arrhenius behavior.

I. Introduction

Supercritical water (SCW) has become an intensively studied medium due to a range of possible applications. It is well-established that supercritical water oxidation (SCWO) is a powerful way to destroy hazardous compounds thanks to the high solubility it affords to both organics and O_2.[1−6] It is less well-known that supercritical water is widely used as the heat transfer medium in gas fired power plants. New designs for more efficient water cooled nuclear reactors using primary cooling loop temperatures and pressures over the critical point of water (374.2 °C, 221 bar) were proposed a few years ago.[7−9] A major unknown is the effect of the radiation on corrosion rates under these conditions. Mostly because of the difficulty of the experiments, chemistry of irradiated water up to supercritical conditions remains poorly defined. In recent years several groups have taken up the challenge to make radiolysis measurements in this regime.[10−16]

In the primary species resulting from the radiolysis of water, hydrated electrons (e_{hyd}^-) and hydroxyl radicals ($OH^•$) are of great importance due to their wide-ranging and complex chemistries.[17] It is therefore of fundamental interest to study and describe their individual reactivities and roles in water radiolysis up to supercritical conditions. Though hydrated electrons are easily measured by their intense absorption in the near IR,[18] $OH^•$ radicals absorb only weakly in the UV. For measurements of $OH^•$ reaction rates, it would be convenient to find a stable molecule whose reaction with $OH^•$ results in a strongly absorbing and reasonably long-lived free radical product. Then other reactions of $OH^•$ could be measured by competition techniques. Nitrobenzene has been used for this purpose,[11,19] but we have found that above 300 °C its extremely fast reaction with hydrated electron and the fast second-order decay of the product radicals makes nitrobenzene difficult to use.[20]

This paper explores the use of phenol as a scavenger for $OH^•$ radicals. Many studies, using different techniques, have been conducted on the reaction of $OH^•$ radicals with phenol in aqueous solutions or in the gas phase,[6,21−38] but the reaction mechanisms or the reaction rate constants are still far from being clearly established. Very recently, a study of the β/γ radiolysis of phenol aqueous solutions up to 400 °C has been reported. The study determined the G values for product formation and phenol consumption, showed transient spectra and proposed a reaction mechanism of the γ-radiolysis of phenol solutions.[16]

It is now well-established that, although the formation of phenoxyl radical is thermodynamically favored,[39] the reaction of $OH^•$ radical by addition to the ring of phenol leads to the formation of dihydroxycyclohexadienyl radicals called "OH-adducts":

$$C_6H_5OH + OH^• \rightarrow {}^•C_6H_5(OH)_2 \quad (1)$$

Hydrogen atoms ($H^•$) formed in the radiolysis of water also react with phenol to yield hydroxycyclohexadienyl radicals, named "H-adducts":

$$C_6H_5OH + H^• \rightarrow {}^•C_6H_6OH \quad (2)$$

The OH-adduct formed then undergoes spontaneous or acid/base-catalyzed loss of a water molecule to yield phenoxyl radical:[22,40,41]

$${}^•C_6H_5(OH)_2 \rightarrow C_6H_5O^• + H_2O \quad (3)$$

The kinetics of the phenoxyl radical formation as well as product analysis studies have shown evidence that more than one OH-adduct isomer is formed by reaction 1: at room temperature the OH-addition to the ring preferentially takes place at the ortho (48%) and the para (36%) positions, whereas meta and ipso positions account for minor (about 8% each) proportion.[26,27,42−44] Moreover, the fraction of ipso-OH-adduct is not distinguishable from direct H-abstraction by the $OH^•$ radical that represents a direct way of formation of phenoxyl radical:

$$C_6H_5OH + OH^• \rightarrow C_6H_5O^• + H_2O \quad (4)$$

* To whom correspondence should be addressed. Phone: +1 574 631 5561. Fax: +1 574 631 8068. E-mail: bartels@hertz.rad.nd.edu.

10.1021/jp0665325 CCC: $37.00
Published on Web 02/21/2007

In the present article that follows a previous work on nitrobenzene,[19] we report our results concerning kinetics of the reaction of the $OH^{\bullet}$ radical with phenol. A detailed analysis of the kinetics observed at 330 nm is exposed, leading to the elucidation of the reaction scheme and to the estimation, as a function of the temperature up to supercritical conditions, of the reaction rate constants required to fit the data. The information complements and enhances the recent product study of Miyazaki et al.[16] to provide a more complete picture of aqueous phenol radiation chemistry.

II. Experimental Section

Electron pulse radiolysis/transient absorption experiments were performed with the 8 MeV Titan Beta (model TBS-8/16-1S) linear accelerator of the Notre Dame Radiation Laboratory, using pulses varying from 3 to 10 ns to select different doses. The corresponding generated aqueous radical concentrations were typically 4−10 μmol L^{-1} per pulse. Analyzing light was supplied by a 75 W xenon arc lamp pulsed for ∼300 μs. The lamp pulse was timed so that the electron pulse coincided with the flattest and most stable part of the lamp flash. The light was then dispersed in a monochromator (SPEX 270M) and detected by a photomultiplier (Hamamatsu R955) coupled to an oscilloscope (Lecroy LC6840DXL) that acquired data. Data handling and the fits were carried out using the Igor Pro 5.0 software (Wavemetrics Inc., Lake Oswego, OR).

The sample cell was a hastelloy C-276 home-designed high-pressure high-temperature flow cell with 3 mm thick sapphire windows, an optical path length of 1.1 cm, inner diameter of 4 mm, and a volume of 0.13 mL. The cell is an improvement on a design published previously,[14] but using the same basic principles. One side of the cell was cut away to a minimum 2 mm hastelloy thickness to provide access for the 8 MeV electron beam. Tests indicated that the geometry affords a very uniform initial excitation. For all the experiments, the concentration of phenol in the sample was set by controlling the phenol stock solution flow rate relative to the pure water flow rate by the use of two independent HPLC pumps (Alltech 301). After the solutions mixed in a tee, they flowed through a preheater of hastelloy tubing wrapped around a cartridge heater that was in thermal contact with the cell body. Additional cartridge heaters were inserted into corners of the cell body to compensate heat loss. The cell and preheater were thermally insulated with 2.5 cm thick calcium sulfate board. Water temperatures at the cell inlet and the cell outlet were measured by thermocouples (Omega KQIN series) inserted into the flow via tee fittings. The inlet and outlet temperatures must match, or scattering of the analyzing light is very severe. After exiting the cell, water was cooled to room temperature in a coil of tubing immersed in a water bath, and pressure was measured with a piezoelectric pressure transducer (Omega PX02 series). Finally, the solution passed through a length of stainless steel capillary tubing that restricted the system output flow to provide back-pressure control. This capillary tubing was immersed in a bath whose temperature was adjusted to regulate the viscosity of the solution. With a fixed total flow rate controlled by the HPLC pumps, this viscosity regulation was used to typically adjust the pressure in the cell to 250 bar. Pressure stability was enhanced with the help of two diaphragm pulse dampeners on each pump, which diminished the pressure oscillation caused by HPLC pump pistons. The total system flow rate was 3.0 mL/min, and after each phenol concentration change, the system was flushed roughly 2 min to ensure enough time for sample renewal into the flow tubing and the cell. Normal system stabilities were ±0.3 °C and ±0.3 bar.

Phenol of 99+% purity was purchased from Aldrich and was used without further purification. Sample solutions were prepared by dissolving the appropriate amount of phenol in ASTM type I purified water (18.2 MΩ cm, H_2Only cartridge and UV purification system). Reservoirs containing pure water and phenol solutions were initially saturated with N_2O or N_2O/O_2 (4/1 v/v) mixture for ∼30 min and then kept slightly bubbled with the same gas during the experiments. N_2O was used to rapidly convert hydrated electrons into $OH^{\bullet}$ radicals:[45]

$$N_2O + e_{hyd}^{-} \rightarrow O^{\bullet -} + N_2 \quad (5)$$

$$O^{\bullet -} + H_2O \rightarrow OH^{-} + OH^{\bullet} \quad (6)$$

Because k_5 was reported as 9.1×10^9 L mol^{-1} s^{-1} and k_6 as 1.0×10^8 L mol^{-1} s^{-1} at room temperature,[17] the conversion occurred with a ∼10 ns delay, roughly the time resolution of the experimental setup. Under these conditions, the total yield of $OH^{\bullet}$ was nearly doubled to reach the value of $G = 5.9$ (in radicals per 100 eV energy absorbed),[46] representing ∼90% of the total primary radicals. Thus, the $OH^{\bullet}$ radicals were the main reactive species in the observed time scale. The remaining 10% were $H^{\bullet}$ atoms, which we will find cannot be ignored at high temperature.

In a second set of experiments, a mixture of N_2O (80%) and O_2 (20%) was used to quickly scavenge $H^{\bullet}$ atoms, in addition to the hydrated electrons conversion by N_2O, thanks to

$$H^{\bullet} + O_2 \rightarrow HO_2^{\bullet} \quad (7)$$

Because k_7 was estimated earlier to be 2.1×10^{10} L mol^{-1} s^{-1},[17,47] this conversion was fast enough to ensure the disappearance of $H^{\bullet}$ atoms as a reactive species in the concerned experiment. As these studies were dedicated mostly to $OH^{\bullet}$ scavenging reactions, we decided not to add KOH or buffers into the samples to prevent any interaction with them.

III. Results and Data Analysis

In this part, we first present the experimental results of the $OH^{\bullet}$ radical reactivity with phenol under N_2O atmosphere. Then we expose the results obtained in the second set of experiments done under a mixture of N_2O and O_2 atmosphere. We finally discuss the kinetic model used to fit the data, and the reaction rate constants resulting from this fitting. We also discuss the consistency of these results in light of the comparison between different experimental conditions, pointing out agreement and disagreement with previously published studies.

A. Experiments under N_2O Atmosphere. Because of its deep UV absorption combined with a low extinction coefficient ($\epsilon_{235\ nm}$ = 580 L mol^{-1} cm^{-1}),[48] changes in $OH^{\bullet}$ radical concentration are difficult to follow directly. The OH-adducts resulting from $OH^{\bullet}$ radical reaction with phenol have a relatively moderate absorption in the UV, with a maximum around 330 nm ($\epsilon_{330\ nm}$ = 4400 L mol^{-1} cm^{-1})[22,24] that allows one to monitor the concentration evolution of this product rather than the concentration evolution of the $OH^{\bullet}$ radical. As mentioned in the Introduction, the $OH^{\bullet}$ radical addition to phenol can occur in four different positions on the ring, leading to the formation of four OH-adducts isomers (ortho, meta, para, and ipso). Because the absorption spectra of these isomers are not distinguishable, to our knowledge, these radicals are assumed to present the same absorption band in aqueous solutions. Moreover, $H^{\bullet}$ atom addition to phenol gives rise to a H-adduct radical, whose spectrum and absorption coefficient ($\epsilon_{330\ nm}$ =

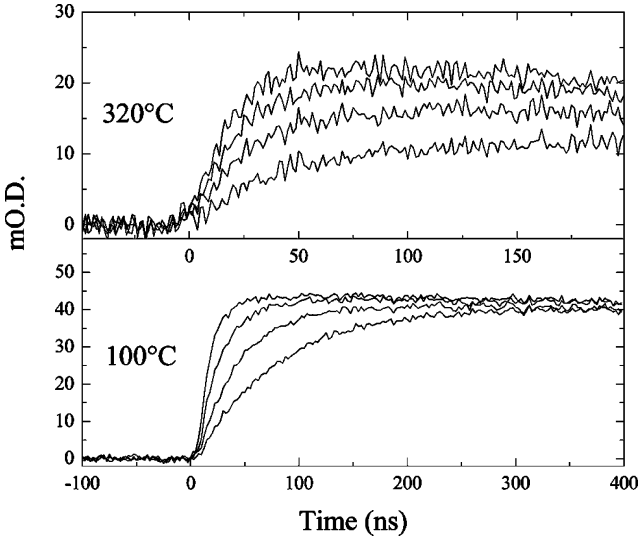

Figure 1. Absorption signals at 330 nm in aqueous solution of phenol at 100 °C (bottom) and 320 °C (top) under N_2O atmosphere. Phenol concentrations are 0.5, 1.0, 2.0 and 4.0×10^{-3} mol L^{-1}, corresponding to the longest through shortest rise times, respectively. Note the two different time scales.

3800 L mol^{-1} cm^{-1})[22] are very similar to the one of the OH-adduct, in accordance with the traditional observation that aromatic molecules display similar absorption spectra for both the $OH^•$ and $H^•$ radical complexes at room temperature.[21,22,49−52] We thus have chosen to follow the kinetics at 330 nm. As phenol is in excess compared to $OH^•$ radicals (phenol concentrations ranged from 5.0×10^{-4} to 8.0×10^{-3} mol L^{-1}, and initial $OH^•$ radical concentrations upon radiolysis were from 4.0×10^{-6} to 1.0×10^{-5} mol L^{-1}), their reaction could be expected to follow a pseudo-first-order kinetics.

Hydroxyl radical scavenging by phenol was carried out as a function of temperature up to 380 °C, at a pressure of 250 bar, except at 380 °C where a measurement of the density dependence (pressure ranging from 215 to 275 bar) was conducted. Both the absorption rise in the first microsecond and the signal decay on longer timescales were recorded. A comparison of the signal rise kinetics for various phenol concentrations is given in Figure 1 for 100 and 320 °C. At 100 °C, the absorption signals at 330 nm obtained for different concentrations of phenol all reach the same plateau, indicating complete scavenging of the available $OH^•$. This is clearly not the case at 320 °C (or other temperatures above 200 °C), where the same phenol concentrations lead to individual plateaus. Changing the dose and corresponding initial radical concentration had no effect on the shape of the kinetics. To explain and fit this behavior, we are forced to postulate an equilibrium at elevated temperatures between free $OH^•$ radicals and the OH···phenol adduct. The signal rise is therefore mainly described with the following first-order reaction set:

$$C_6H_5OH + OH^• \rightarrow {}^•C_6H_5(OH)_2 \quad (1)$$

$$C_6H_5OH + H^• \rightarrow {}^•C_6H_6OH \quad (2)$$

$${}^•C_6H_5(OH)_2 \rightarrow C_6H_5O^• + H_2O \quad (3)$$

$${}^•C_6H_5(OH)_2 \rightarrow OH^• + C_6H_5OH \quad (8)$$

We were unable to fit the data with any other reasonable mechanism. In fact, other evidence supports the validity of reaction 8. The OH-addition reactions to phenol, benzene or other aromatics are known to be reversible in the gas phase,[35,36,53−58] and an equilibrium has even been proposed in solution for benzene.[59]

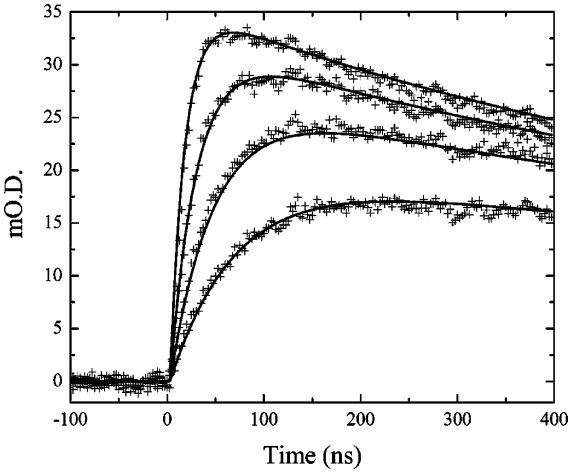

Figure 2. Sample fitted data for $OH^•$ radical scavenging by phenol at 275 °C and 250 bar in N_2O atmosphere. Phenol concentrations are 0.5, 1.0, 2.0 and 4.0×10^{-3} mol L^{-1}, corresponding to the longest through shortest rise times.

TABLE 1: Parameters of the Fourth-Degree Polynomial Expressions Used To Calculate Yields of Primary Species as a Function of Temperature (°C) Up to 380 °C (Only Valid at 250 Bar; See Text)

	G (molecule/100 eV) $= a*T^4 + b*T^3 + c*T^2 + d*T + e$				
	a	*b*	*c*	*d*	*e*
$H^•$	6.262×10^{-10}	-3.861×10^{-7}	9.046×10^{-5}	−0.006944	0.67293
$OH^•$		3.112×10^{-8}	-1.995×10^{-5}	0.008211	2.7991
e_{hyd}^-	-3.678×10^{-10}	2.291×10^{-7}	-5.675×10^{-5}	0.00885	2.5704

A sample of fitted signal rise using this mechanism at 275 °C is shown in Figure 2. The shortest and the longest rise times correspond to the highest and the lowest phenol concentrations, respectively. The increase in the absorption is mostly attributed to the formation of dihydroxycyclohexadienyl radicals that produce the transient absorption at 330 nm. However, on the basis of both published radiolysis yield measurements and recent product yield measurement made in this laboratory,[10,13,60−62] $H^•$ atoms should account for up to 20% at 300 °C, the proportion being smaller at lower temperatures. Therefore the contribution of H-adducts absorption should be taken into account as the relative radiation yield of $H^•$ atoms increases substantially with temperature.[10] The G values for $OH^•$ were calculated on the basis of data reported previously by Lin et al. up to 350 °C.[13] From the total $G(OH^• + e_{hyd}^- + H^•)$ reported in that paper, we subtracted the sum of $G(e_{hyd}^-)$ and $G(H^•)$ determined in our laboratory from gas product analysis in irradiated N_2O-saturated aqueous solutions of phenol and EtOH-d_6,[61] respectively. Parameters of the interpolating polynomial expressions used here to calculate $H^•$ atom, $OH^•$ radical, and hydrated electron yields as a function of temperature are given in Table 1 (these expressions are considered valid up to 380 °C, but only for 250 bar pressure).

Figure 3 presents the observed and fitted decay kinetics of the 330 nm absorption on a longer time scale as a function of temperature. Note the decrease in initial absorption maximum resulting from the equilibrium formed from reactions 1 and 8 (as well as the decreasing density). On the basis of the earlier cited studies dealing with the $OH^•$ radical reaction with phenol, the following additional reactions have been employed to fit the full kinetics at 330 nm:

$$2^{\bullet}C_6H_5(OH)_2 \rightarrow \text{products} \quad (9)$$

$$2^{\bullet}C_6H_6OH \rightarrow \text{products} \quad (10)$$

$$^{\bullet}C_6H_5(OH)_2 + {}^{\bullet}C_6H_6OH \rightarrow \text{products} \quad (11)$$

$$2C_6H_5O^{\bullet} \rightarrow \text{products} \quad (12)$$

$$^{\bullet}C_6H_5(OH)_2 + C_6H_5O^{\bullet} \rightarrow C_6H_5OH + \text{product} \quad (13)$$

$$^{\bullet}C_6H_6OH + C_6H_5O^{\bullet} \rightarrow 2C_6H_5OH \quad (14)$$

$$^{\bullet}C_6H_6OH \rightarrow C_6H_6 + OH^{\bullet} \quad (15)$$

The formation and decay of the H-adduct radical is explicitly included in the model, and its contribution to the absorption is taken into account according to its reported absorption coefficient. Indeed, when we initially attempted to fully describe the kinetics of the reactions without H-adduct chemistry, we were unable to fit the data corresponding to the absorption decay. This is because the OH-adduct decays via first-order reaction 3 to the more weakly absorbing phenoxyl radical, leaving the H-adduct as the strongest absorbing species. The remaining absorption at long time (the decay kinetics do not fall to zero in the measured time scale, as can be observed in Figure 3) is attributed to the small absorption of the phenoxyl radical. For fitting we have assumed an absorption coefficient of ~500 L mol^{-1} cm^{-1} at 330 nm, according to its previously reported absorption spectrum.[24,29,32,63,64] Final products that are formed, mainly dihydroxybenzenes,[16] do not significantly absorb at this wavelength.[24,65]

A decay of the phenoxyl radical has been included in the fitting model via a second-order self-recombination (reaction 12), as proposed in several publications describing various phenoxyl radical chemistries.[24,29,37,66,67] Crossed recombination reactions with the adducts (reactions 13 and 14) have also been considered because there is no evidence that these reactions are slow enough to be ignored. To complete the set of reactions needed to fit the absorption decay, we have also considered the second-order recombination of OH-adduct radicals (reaction 9), of H-adduct radicals (reaction 10) and the crossed recombination of the two adducts (reaction 11), in accordance with previous studies.[16,22,26,34,37] Moreover, these recombination reactions lead to the re-formation of phenol, which is consistent with the relatively moderate yield of phenol consumption observed in the study of Miyazaki, et al.[16] It is certainly impossible to extract all of these second-order rate constants by fitting the single wavelength, as they probably all have similar magnitudes. Instead, we make the simplifying assumption/approximation that all of them have the same value, and fit this average value.

Finally, to obtain a full agreement between the fitting and the data, it appeared to us that another first-order channel of decay for the H-adduct was necessary at higher temperature, especially above 300 °C. In accord with the experimental observation of the formation of benzene at high temperature in the radiolysis of phenol aqueous solutions,[16] we have considered a first-order dissociation of H-adduct radicals (reaction 15) giving benzene and the $OH^{\bullet}$ radical. This set of reactions and yields gives an excellent accounting of the full kinetics at 330 nm over the entire temperature range, as can be seen in Figure 3.

We should emphasize that our kinetics model is consistent with the pulse radiolysis data presented in the recent study of

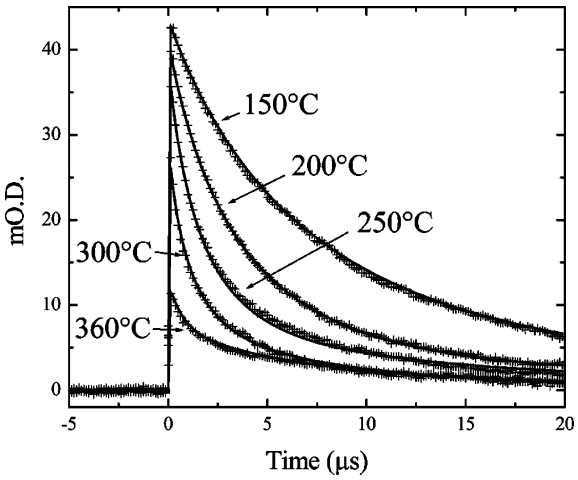

Figure 3. Sample fitted data showing the 330 nm absorption growth and decay in an aqueous solution of phenol (4.0×10^{-3} mol L^{-1}) under N_2O atmosphere at 150, 200, 250, 300 and 360 °C, corresponding to the slowest through the fastest decay, respectively.

Miyazaki et al.[16] Figure 3 of ref 16 shows transient spectra from 270 to 600 nm, obtained at 1 μs following pulse radiolysis of N_2O-saturated 1.0 mM phenol solutions from room temperature to 400 °C. Miyazaki et al. considered that the adduct spectra and extinction coefficients must be changing with temperature because the OH-adduct absorption at 330 nm becomes much weaker at high temperature.[16] The signal amplitudes in this figure at 330 nm are very similar to those of our own study. We have been able to obtain a consistent global fit using the room-temperature extinction coefficients. At elevated temperature, the signals become dominated by the H-adduct in 1.0 mM solution because the OH-adduct is present only in low concentrations. Thus, we believe the 330 nm extinction coefficients change very little with temperature (probably less that 20%). Whatever temperature change of extinction coefficients is present can have only minor impact on the pseudo-first-order rate constants we derive but will affect the second-order decay rate constants in direct proportion to the error. A further constraint on the relative absorbance of OH- and H-adducts is provided by the study with dissolved O_2, described below.

The main discrepancy in our kinetics scheme is the omission of a direct reaction of H-abstraction from phenol by the $OH^{\bullet}$ radical, as proposed in $OH^{\bullet}$ reactions to aliphatic alcohols and observed in Raman experiments:[68,69]

$$C_6H_5OH + OH^{\bullet} \rightarrow C_6H_5O^{\bullet} + H_2O \quad (4)$$

Mvula et al. claimed that this reaction is not distinguishable from the formation of the ipso-OH-adduct, representing a total of ~8% of the total reaction of $OH^{\bullet}$ radicals with phenol.[34] Roder et al. estimated the rate constant of reaction 4 to be between 1.5 and 1.8×10^6 s^{-1} in acidic solutions,[41] compared to rate constant values estimated higher than 10^5 s^{-1} in previous studies.[22,40] So, we performed a few measurements at 400 nm where the only absorbing species is the phenoxyl radical (ϵ_{400nm} = 2900 L mol^{-1} cm^{-1}).[64] To properly fit the absorption growth, we needed to use reaction 4 in addition to the kinetic scheme proposed. Thus we are in agreement with other experimental proofs of this reaction. The results of the fit of the 400 nm absorption signals are shown in Figure 4, and we obtained a good agreement with experimental data. However, the influence of reaction 4 on the 330 nm absorption signals is almost undetectable, due to the small proportion (no more than 8%) combined with a relatively small absorption coefficient for phenoxyl radical. When attempting to take into account this

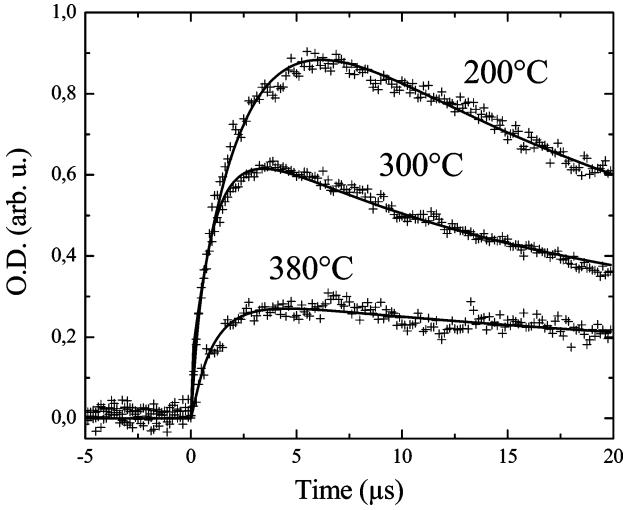

Figure 4. Absorption signals at 400 nm, corresponding to phenoxyl radical formation, recorded at 200, 300, and 380 °C in an aqueous solutions of phenol (4.0×10^{-3} mol L^{-1}) under a N_2O atmosphere.

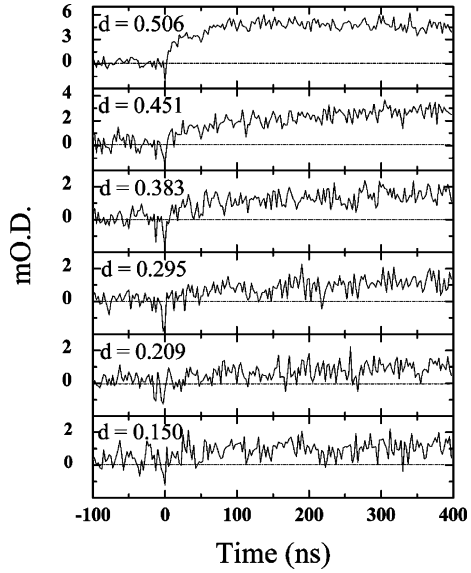

Figure 5. Absorption signal at 330 nm recorded at a pressure of 215, 230, 235, 240, 250, and 275 bar, from bottom to top, in an aqueous solution containing 4.0×10^{-3} mol L^{-1} of phenol at 380 °C.

reaction, whatever the temperature, it appeared that its rate constant simply combined with those of reaction 3 to always give the same global formation of phenoxyl radicals. So, we decided that the apparent role of this reaction can reasonably be neglected in our fitting model for data at 330 nm, as the recent study published by Miyazaki et al. also does.[16]

Finally, we performed experiments to evaluate the density dependence of the reaction rate constant of $OH^\bullet$ radicals with phenol in supercritical water. For that purpose, we measured the absorption signal at six different pressures ranging from 215 to 275 bar at a fixed temperature of 380 °C. Because this represents a region where water is highly compressible (Figure 5),[70] the corresponding densities range from 0.15 to 0.50 g/cm^3. The signals obtained at 330 nm are illustrated in Figure 5. The absorption becomes weaker at lower densities first because less radiolysis energy is absorbed. The rise time becomes slower because the absolute density of the phenol scavenger becomes smaller as well. And even assuming the equilibrium does not change, the lower phenol concentration favors the free $OH^\bullet$ side of the equilibrium. Although these factors can be countered with higher dose and somewhat higher phenol concentrations to increase the signal, the incomplete scavenging clearly makes this system more difficult to use for $OH^\bullet$ competition measurements than one would like.

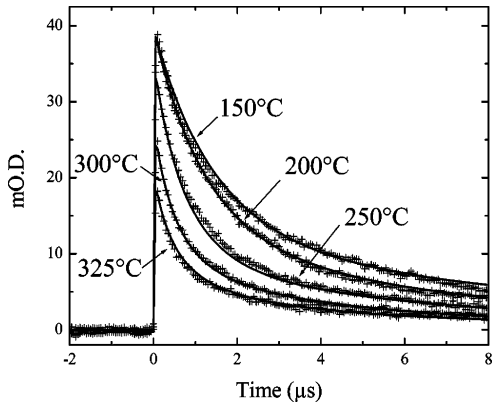

Figure 6. Sample fitted data showing the 330 nm absorption growth and decay in an aqueous solution of phenol (4×10^{-3} mol L^{-1}) under a N_2O-O_2 atmosphere at 150, 200, 250, 300, and 325 °C, corresponding to the slowest through the fastest decay, respectively.

B. Experiments under N_2O-O_2 Atmosphere. In an attempt to avoid $H^\bullet$ atom reactions, we performed a second set of experiments under the atmosphere of a 4:1 mixture of N_2O and O_2. So, in addition to the fast conversion of hydrated electrons to $OH^\bullet$ radicals, $H^\bullet$ atoms are quickly scavenged (assuming a rate constant of 2.1×10^{10} L mol^{-1} s^{-1})[17] by oxygen, thanks to reaction 7. The second major consequence of the presence of oxygen in the system is the faster decay, compared to pure N_2O atmosphere, of the initial absorption of the OH-adduct radicals at 330 nm, as shown in Figure 6 (note the different time scale compared to Figure 3). Actually, it is known that these radicals are being converted to corresponding peroxyl radicals (and probably different isomers) thanks to reaction 16:[24,26,34]

$$^\bullet C_6H_5(OH)_2 + O_2 \rightarrow C_6H_5(OH)_2O_2^\bullet \qquad (16)$$

The peroxyl radical formed in this reaction is then known to decompose mainly unimolecularly to form products (dihydroxybenzenes) by the elimination of an $HO_2^\bullet$ radical:

$$C_6H_5(OH)_2O_2^\bullet \rightarrow C_6H_4(OH)_2 + HO_2^\bullet \qquad (17)$$

The relative efficiency of this elimination leaves little room for a hypothetical reverse oxygen elimination, unlike other hydroxycyclohexadienyl radicals.[34,71]

Even if this peroxyl radical presents a weaker absorption at 330 nm than the OH-adduct radical, it appeared to us that its contribution to absorption could not be neglected, as its absorption coefficient at 330 nm is ~30% that of the OH-adduct radical.[24] So we assumed and included in the fitting procedure a value of $\epsilon_{330nm} = 1400$ L mol^{-1} cm^{-1} for the peroxyl radical. The results of the experiments and of the corresponding fittings are illustrated in Figures 6 and 7. We observe a faster decay of the absorption signal compared to the previous due to reaction 16 and a very satisfying agreement has been obtained with our fitting model, keeping the rate constants for reactions 1, 3, 8, 9, 12, and 13 the same compared to pure N_2O atmosphere, and removing reactions 2, 10, 11, 14, and 15 corresponding to $H^\bullet$ atom reactions. One can point out that the time range for the fitting of the absorption decay is shorter in this second set of experiments than in the previous one in the case of pure N_2O atmosphere (10 μs against 25 μs). This can be explained, first, by the fact that in the presence of oxygen, the kinetics of the decay are faster due to reaction 16 but, second, and to be fully

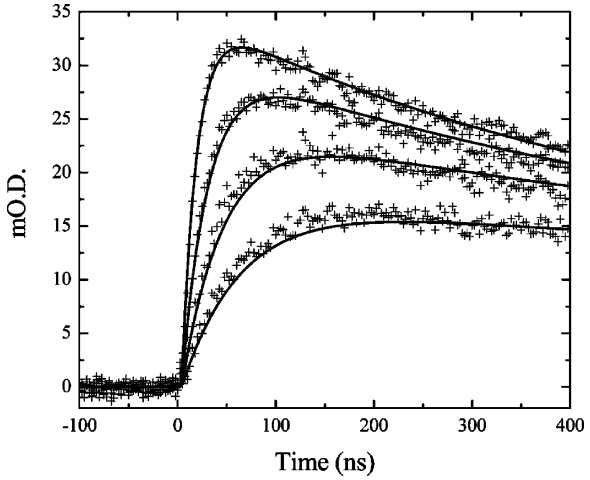

Figure 7. Sample fitted data for $OH^{\bullet}$ radical scavenging by phenol at 275 °C and 250 bar in a N_2O-O_2 atmosphere. Phenol concentrations are 0.5, 1.0, 2.0, and 4.0×10^{-3} mol L^{-1}, corresponding to the longest through shortest rise rates.

TABLE 2: Fitted Rate Constants for the Reaction of Phenol with the Hydroxyl Radical (Reaction 1) and the Hydrogen Atom (Reaction 2)[a]

	rate constant, (L mol^{-1} s^{-1}) $\times 10^{-10}$	
T (°C)	reaction 1	reaction 2
21	0.841 ± 0.042	0.124 ± 0.006
100	2.45 ± 0.12	0.622 ± 0.031
150	2.75 ± 0.14	1.28 ± 0.06
200	2.50 ± 0.13	2.54 ± 0.13
225	2.34 ± 0.12	2.95 ± 0.15
250	2.15 ± 0.11	2.62 ± 0.13
275	1.80 ± 0.09	2.30 ± 0.11
300	1.33 ± 0.07	1.96 ± 0.10
320	1.14 ± 0.06	1.56 ± 0.08
340	1.31 ± 0.07	1.03 ± 0.06
360	1.38 ± 0.07	0.726 ± 0.036
380	1.62 ± 0.16	0.548 ± 0.054

[a] Errors represent one standard deviation of the fitted parameters. Additional systematic error may influence the results (see text).

honest, because we failed to obtain a completely satisfying agreement for a 25 μs time window. Indeed, the decomposition of peroxyl radicals produces highly reactive species such as $HO_2^{\bullet}$ radicals, which then yield $O_2^{\bullet-}$, that can react with the radicals already present in the medium. Moreover, oxygen can involve a large number of reactions in the microsecond time scale, for example with phenoxyl for which there is a controversy in the literature giving no reaction[67] as well as a rate constant[24] of $\sim 10^7$ L mol^{-1} s^{-1}. So we reasonably restrict the time window of the fitting to the first 10 μs to focus our attention on the first species formed, directly linked to the reaction of $OH^{\bullet}$ radicals and phenol, and not increase the number of reactions and the complexity of the kinetic model. And, finally, this choice leads to a very good and logical agreement between fits and data obtained in anoxic conditions (see Figures 6 and 7).

C. Reaction Rate Constants. The two sets of experiments presented in previous sections gave results that match together in a very good way, reinforcing our confidence in the kinetic scheme proposed. The results reported in Table 2 for the OH- and H-addition to phenol represent an average of the fitted rate constants obtained for the four phenol concentrations and two or three doses run at each temperature. The associated error bars represent one standard deviation of this average. The error bars of 5 or 10% given for the additional rate constants listed in Tables 3 and 4 correspond to the average of values obtained for different calculations, varied by changing the number of free parameters, fitting different repetitive experiments, and requiring agreement between experiments with and without O_2. Uncertainty in the ratio of extinction coefficients for H- and OH-adducts is strongly constrained by the fitting of the two separate experiments and by the several parallel fits in different conditions. Additional systematic errors from extinction coefficients or G values used may certainly be present, but we do not believe they will exceed 20%.

TABLE 3: Fitted Rate Constants for Reactions 3 and 8−15 as a Function of Temperature[a]

	rate constants (L mol^{-1} s^{-1})			
T (°C)	reaction 3 $\times 10^{-5}$ [b]	reaction 8 $\times 10^{-6}$ [b]	reactions 9−14 $k_{eff} \times 10^{-10}$	reaction 15 $\times 10^{-4}$
21	0.146	0.221	0.079	
100	0.772	0.456	0.121	
150	1.32	0.915	0.278	
200	2.52	2.29	0.870	
225	3.42	3.21	1.19	
250	5.32	7.27	1.66	
275	8.26	11.5	2.45	
300	14.8	24.9	3.42	1.67
320	21.1	34.7	4.63	4.81
340	31.5	53.8	5.50	6.41
360	49.1	71.4	4.03	8.44
380	36.8	68.2	3.48	8.86

[a] Typical variation in the fitted parameters is ±5% up to 340 °C, and ±10% in supercritical conditions. Additional systematic error may influence the results (see text). [b] Note: values below 150 °C are to be taken with precaution due to the low sensitivity of the fitting quality to these rate constants in this range of temperature.

TABLE 4: Fitted Rate Constants for Reactions 16 and 17 Relative to the Formation and the Decay of the Peroxyl Radical as a Function of Temperature[a]

	rate constants (M^{-1} s^{-1})	
T (°C)	reaction $\times 10^{-9}$	reaction $\times 10^{-5}$
21	1.49	0.438
100	1.77	0.812
150	2.05	1.32
200	2.32	1.76
225	2.76	1.96
250	3.56	2.20
275	3.94	2.61
300	4.90	3.08
325	5.97	3.21
350	7.08	1.63

[a] Typical variation in the fitted parameters is ±5%. Additional systematic error may influence the results (see text).

An Arrhenius plot of the extracted rate constants of reaction of the $OH^{\bullet}$ radical with phenol is shown in Figure 8, and the corresponding numbers are given in Table 2. The shape of this plot is similar to the one obtained with nitrobenzene,[11,19] with only a factor of 3 variation over the full temperature range. The rate constant increases continuously from room temperature to 150 °C (to reach a value 3 times bigger than at room temperature) and then decreases with temperature up to 320 °C, to finally increase again as the critical temperature is approached and passed. The reaction rate constant at room temperature is found to be $(8.41 \pm 0.42) \times 10^9$ L mol^{-1} s^{-1}. This represents the main discrepancy of our results compared to previous studies, especially the often cited study by Land and Ebert done in 1967, which indicates a rate constant of 1.4×10^{10} L mol^{-1} s^{-1}.[22] However, a careful reading of this article reveals that the latter value corresponds to a pH of 7.4−7.7, and a value of 1.06×10^{10} L mol^{-1} s^{-1} is indicated for a pH of 6−7. Having

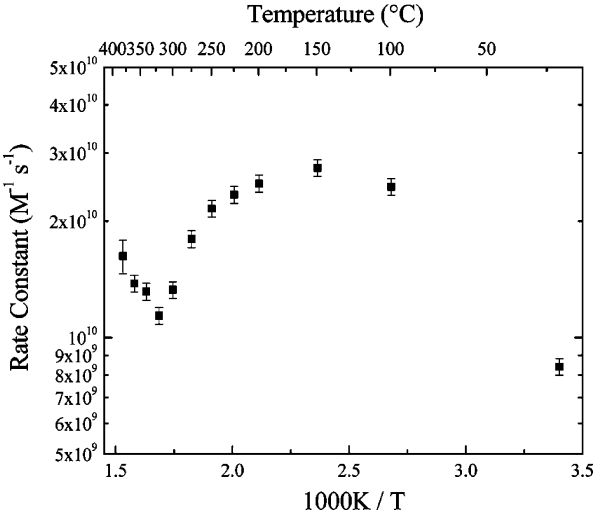

Figure 8. Arrhenius plot for the reaction of phenol with OH• radicals.

in mind that the pH of deionized water is below 7, the disagreement becomes weaker. Finally, if we consult the widely cited Buxton et al. review on rate constants for hydrated electrons, hydrogen atoms and hydroxyl radicals,[17] we realize that there are only three reported rate constants, including one of 6.6×10^9 L mol^{-1} s^{-1} obtained by Field et al. in 1982.[29]

To confirm the rate constant we obtain, we finally performed a few experiments of competition kinetics in a system containing phenol at a fixed concentration of 5.0×10^{-3} mol L^{-1}, under pure N_2O atmosphere and different concentrations of ethanol. The most common method to analyze such competition kinetic experiments, employed and improved for a while,[72] is simply to measure the ratio of absorbance for different ratios of concentration of the two competitors, providing that the product of the competitor does not absorb at the wavelength of observation:

$$\begin{cases} OH^\bullet + S_1 \xrightarrow{k_1} \text{absorbing products} \\ OH^\bullet + S_2 \xrightarrow{k_2} \text{nonabsorbing products} \end{cases}$$

$$OD_0/OD = 1 + (k_2[S_2]/k_1[S_1]) \qquad (18)$$

where S_1 and S_2 are scavenger #1 (phenol in our case) and scavenger #2 (ethanol in our case), respectively, and OD_0 represents the optical density in absence of scavenger S_2. Relative rate constants can therefore be determined by plotting OD_0/OD as a function of the ratio $[S_2]/[S_1]$. The result of this experiment is illustrated in Figure 9, representing the absorption signal at 330 nm without and with increasing concentration of ethanol, at room temperature. The inset of the figure shows the plot of the absorbance ratios versus concentration ratios, which is perfectly linear. The slope of the plot is 0.2235, and with the rate constant of the reaction between the OH• radical and phenol (Table 2), that leads to a rate constant for the reaction of the OH• radical and ethanol of 1.88×10^9 L mol^{-1} s^{-1}, in perfect agreement with the accepted value of 1.9×10^9 L mol^{-1} s^{-1}.[17] So we conclude that our results are absolutely reasonable.

The rates of addition of OH• radicals to several substituted benzenes have been investigated up to 200 °C by Ashton et al.[32] OH• addition to nitrobenzene has been investigated up to 400 °C by Feng et al.,[11] and also by Marin et al.[19] In all of these cases, the rate constant changes only a small amount from room temperature and shows some decrease above 150 °C. In the nitrobenzene case it was found that the rate constant

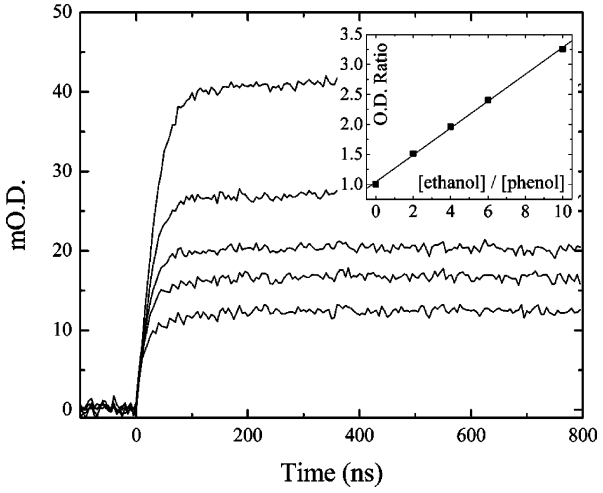

Figure 9. Absorption traces obtained by the radiolysis at room temperature of 5×10^{-3} mol L^{-1} aqueous solutions of phenol containing 0, 0.5, 1.0, 2.0×10^{-2}, and 4.0×10^{-2} mol L^{-1} of ethanol, from top to bottom, respectively. Inset: plot of absorbance ratios vs concentration ratios.

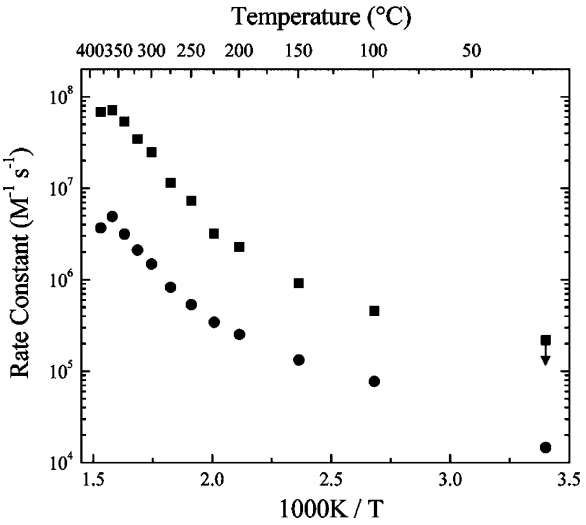

Figure 10. Arrhenius plot for the formation reaction of phenoxyl radicals (reaction 3, circles) and for the reaction giving back reactants (reaction 8, squares) from dihydroxycyclohexadienyl radicals.

suddenly increased above 350 °C, much as we find in this work for phenol. Ashton et al. proposed a mechanism involving fast, ca. diffusion-limited addition of OH• to form an initial "π-adduct".[32] It was postulated that this weakly bound "π-adduct" would then either cross to a more stable σ-bonded "σ-adduct" or fall apart again to the OH• radical and aromatic molecule. Feng et al. demonstrated that this mechanism could explain the increased rate for nitrobenzene at high temperature, due to a large increase in diffusion rates in the near critical region.[11] A similar analysis can rationalize the rate constants for formation of the observed phenol "σ-adduct" at 330 nm. More recently, the "π-adduct" complex has been found in an ab initio study of the reaction of OH• with benzene in the gas phase,[73] which would seem to confirm the validity of the Ashton et al. mechanism.

Figure 10 plots the fitted values for reaction 3 and reaction 8, corresponding to the creation of phenoxyl radical and re-formation of phenol and OH• radical from the OH-adduct, respectively. We wish to emphasize that the rate constants for these reactions and for reaction 1, all first-order or pseudo-first-order, are very robustly determined from the 330 nm absorption

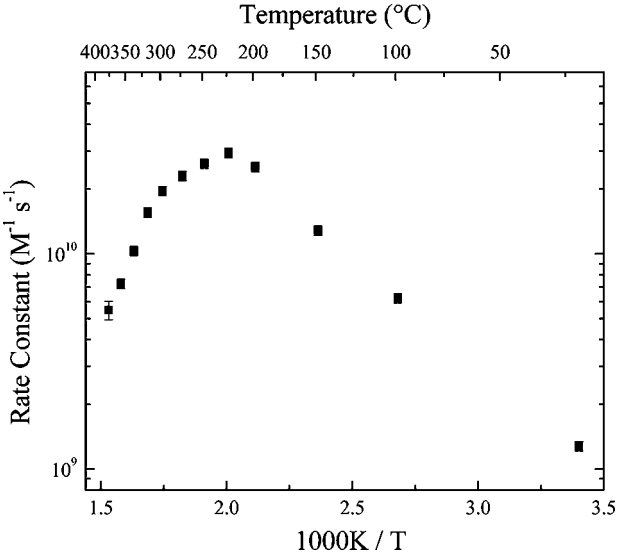

Figure 11. Arrhenius plot for the reaction of phenol with H• atoms.

data independent of assumed yields, extinction coefficients, and even the additional reactions required to fit the second-order decays. The room-temperature value of k_3 (1.46×10^4 L mol^{-1} s^{-1}) is right in the middle of the different rate constants ranging between 1.8×10^3 and 8.0×10^4 L mol^{-1} s^{-1} available in the literature.[22,29,34,37] This reaction is known to be both acid and base catalyzed, which certainly accounts for much of the spread in reported values. The temperature dependences of both reactions are seen to be very similar, with an activation energy of 18 kJ/mol below 200 °C, and a larger activation energy of 48 kJ/mol at higher temperatures. The similarity of the temperature dependences suggests a common root cause. Possibly, it is related to the temperature-dependent pK_a value of the OH-adduct,[69] but we can provide no solid explanation for the temperature dependence at this time. One would suppose that reaction 8 represents the reverse reaction of "σ-adduct" formation from "π-adduct" in the Ashton et al. mechanism discussed above. The similarity of reactions 3 and 8 then suggests to us that the formation of phenoxyl radical occurs via the π-adduct. This could be tested with future experiments as a function of pH.

Figure 11 presents an Arrhenius plot of the extracted rate constants of reaction of the H• atom with phenol corresponding to the values of Table 2. The evolution of the rate constant shows a quasi-linear increase from room temperature to 225 °C, reaching its maximum below the critical point, followed by a decrease at higher temperatures. The value obtained at room temperature (1.24×10^9 L mol^{-1} s^{-1}) agrees well with the 1.2×10^9 L mol^{-1} s^{-1} previously published value.[64] However, the rate constant values below 150 °C result most from the G values for the H• atom assumed for the fit (Table 1). In fact, the data are fairly insensitive to the presence of H• below 100 °C. The decrease of the rate constant above 225 °C is startling, but a similar behavior has been observed for the temperature-dependent rate constant of muonium addition to benzene.[12,74] It has been argued that H• atom addition to aromatics will be accelerated, relative to the gas-phase rates, by their unfavorable solvation free energy.[75] That is, attaching the hydrophobic atom to the benzene ring in the transition state will recover virtually all of the H• atom solvation free energy, and accelerate the reaction relative to gas phase by the factor exp[$\Delta G_{hyd}(H^{\bullet})/RT$] (the ΔG_{hyd} for H• atoms is closely approximated by the tabulated numbers for the H_2 molecule).[75] This factor can give rise to a maximum in reaction rate, if it is multiplied by a simple Arrhenius law expression. In the present case, we have divided the measured rate constants by the acceleration factor, but we do not obtain a simple monotonic "gas phase" curve. Additional solvation effects appear to be important in forming the transition state.

To find the best compromise between considering all the possible recombination reactions in which OH- and H-adducts and phenoxyl radicals can be involved (namely reactions 9−14), and limiting the number of free parameters of the fit, we determined an effective second-order rate constant by assuming the same rate constant for all these recombination reactions. The assumption is reasonable in that all of them can be shown to be in the near diffusion-limit regime, all of the reactants are of similar size and diffusion rate, and all except (13) represent a disproportionation via H• atom transfer. However, we do not claim that this procedure will necessarily give a correct rate constant for any of the individual reactions 9−14. And, of course, these rate constants are affected by inaccuracy in the extinction coefficients assumed, which may change with temperature (the ratio of H−H and OH−adduct absorbance seems to be insensitive to temperature, however). Nevertheless, it is important that this effective average rate constant have a physically reasonable value, to give confidence in the overall fitting scheme. The average second-order rate constant as a function of temperature, corresponding to the reactions involved in our modeling, is included in Table 3. In Figure S1 of the Supporting Information we compare these numbers with an estimate of the diffusion limit from the Smoluchowski equation, $k_{diff} = \beta 4\pi RD$, where the spin factor $\beta = {}^1/_4$, reaction distance R is taken as 0.7 nm, and relative diffusion coefficient D is 2.0 $\times 10^{-9}$ m^2 s^{-1} at room temperature, scaled vs temperature by multiplication by T/viscosity. The average second-order decay falls an order of magnitude below the diffusion limit at 100 °C, then approaches it again at higher temperature, but remains in a physically sensible range. At room temperature the average second-order rate (7.86×10^8 L mol^{-1} s^{-1}) is significantly higher than those obtained by Mvula et al. for the pure OH-adducts recombination (1.0×10^8 L mol^{-1} s^{-1})[34] but is in agreement with the value of Miyazaki et al. (6.0×10^8 L mol^{-1} s^{-1}).[16] This value also corresponds quite well with the second-order recombination of phenoxyl radicals as proposed by Field et al. (3.0×10^8 L mol^{-1} s^{-1})[29] or by Micic et al. (6.0×10^8 L mol^{-1} s^{-1}).[24]

Very few studies indicate the rate constant for unimolecular dissociation of H-adducts, but it is generally assumed that this rate constant is small. The value we obtained for reaction 15 corresponds well with the observation made by Miyazaki et al. on the formation of benzene in phenol−N_2O systems only above 300 °C.[16] Concerning the peroxyl radical, both its room temperature formation rate constant ($k_{16} = 1.49 \times 10^9$ L mol^{-1} s^{-1}) and its first-order decay ($k_{17} = 4.4 \times 10^4$ L mol^{-1} s^{-1}) are in agreement with published values,[24,34] and values obtained in our fitting are summarized in Table 4. The decay rate constant is activated with 9.8 kJ/mol activation energy. The formation reaction (O_2 addition to OH-adduct) is well below the diffusion limit and shows little change with temperature until 200 °C is reached.

IV. Conclusions

The rate constants for the reaction of phenol with the hydroxyl radical in water have been measured from room temperature to 380 °C using pulse radiolysis and transient absorption spectroscopy. In parallel, a kinetic model has been designed to describe and fit the evolution of the absorption at 330 nm. The

results, which give a very good agreement between experiments and modeling as well as coherent rate constants at room temperature, highlight the presence of a reverse reaction of OH-addition to the ring of phenol, giving back the reactants. They also show that hydrogen atom addition to the phenol, producing H-adduct radicals, should not be neglected, in particular above 250 °C.

The consistency and the reality itself of the equilibrium have been tested by the application of the modeling scheme to another experimental condition (presence of oxygen), leading to the same good agreement in the results. As a consequence, it has been possible to determine the rate constants for all the reactions involved in the kinetic scheme up to supercritical conditions, which agree well with a recent product study on the same system.[16] The temperature dependence of nearly every reaction rate in the system is non-Arrhenius above 100 °C. Given the absence of strong absorption at 330 nm in low density solutions at 380 °C due to the equilibrium of OH-addition to phenol, it seems clear to us that phenol is not the most suitable competition partner for $OH^{\bullet}$ radical kinetic studies above the critical point of water.

Acknowledgment. We gratefully thank Dr. G. N. R. Tripathi for constructive discussions and useful information and references provided. The research described herein was supported by the Office of Basic Energy Sciences of the Department of Energy. This is contribution no. NDRL 4663 from the Notre Dame Radiation Laboratory.

Supporting Information Available: Figure S1 comparing the average rate for reactions 9−14 with the diffusion limit. This material is available free of charge via the Internet at http://pubs.acs.org.

References and Notes

(1) Shaw, R. W. *Chem. Eng. News* **1991**, *69*, 26.
(2) Sealock, J. L.; Elliott, D. C.; Baker, E. G.; Butner, S. R. *Ind. Eng. Chem. Res.* **1993**, *32*, 1535.
(3) Gopalan, S.; Savage, P. E. *J. Phys. Chem.* **1994**, *98*, 12646.
(4) Krajnc, M.; Levec, J. *AIChE J.* **1996**, *42*, 1977.
(5) Matsumura, Y.; Nunoura, T.; Urase, T.; Yamamoto, K. *J. Hazardous Mater.* **2000**, *73*, 245.
(6) Thornton, T. D.; Savage, P. E. *Ind. Eng. Chem. Res.* **1992**, *31*, 2451.
(7) Dobashi, K.; Kimura, A.; Oka, Y.; Koshizuka, S. *Ann. Nucl. Energy* **1998**, *25*, 487.
(8) *Technology Roadmap for Generation IV Nuclear Energy Systems*; U.S. Department of Energy Nuclear Energy Research Advisory Committee & Generation IV International Forum; U.S. DOE: Washington, DC, 2002.
(9) SCR2000. *Proceedings of The First International Symposium on Supercritical Water Cooled Reactors, Design and Technology*; The First International Symposium on Supercritical Water Cooled Reactors, Design and Technology, 2000, Tokyo, Japan; 2000.
(10) Cline, J.; Takahashi, K.; Marin, T. W.; Jonah, C. D.; Bartels, D. M. *J. Phys. Chem. A* **2002**, *106*, 12260.
(11) Feng, J.; Aki, S. N. V. K.; Chateauneuf, J. E.; Brennecke, J. F. *J. Am. Chem. Soc.* **2002**, *124*, 6304.
(12) Ghandi, K.; Addison-Jones, B.; Brodovitch, J. C.; Kecman, S.; McKenzie, I.; Percival, P. W. *Physica B* **2003**, *326*, 55.
(13) Lin, M.; Katsumura, Y. M., Y.; He, H.; Wu, G.; Han, Z.; Miyazaki, T.; Kudo, H. *J. Phys. Chem. A* **2004**, *108*, 8287.
(14) Takahashi, K.; Cline, J. A.; Bartels, D. M.; Jonah, C. D. *Rev. Sci. Instrum.* **2000**, *71*, 3345.
(15) Lin, M.; Katsumura, Y.; He, H.; Muroya, Y.; Han, Z.; Miyazaki, T.; Kudo, H. *J. Phys. Chem. A* **2005**, *109*, 2847.
(16) Miyazaki, T.; Katsumura, Y.; Lin, M.; Muroya, Y.; Kudo, H.; Taguchi, M.; Asano, M.; Yoshida, M. *Rad. Phys. Chem.* **2006**, *75*, 408.
(17) Buxton, G. V.; Greenstock, C. L.; Helman, W. P.; Ross, A. B. *J. Phys. Chem. Ref. Data* **1988**, *17*, 513.
(18) Bartels, D. M.; Takahashi, K.; Cline, J. A.; Marin, T. M.; Jonah, C. D. *J. Phys. Chem. A* **2005**, *105*, 1299.
(19) Marin, T. M.; Cline, J. A.; Takahashi, K.; Bartels, D. M.; Jonah, C. D. *J. Phys. Chem. A* **2002**, *106*, 12270.
(20) Marin, T. M.; Jonah, C. D.; Bartels, D. M. *Chem. Phys. Lett.* **2003**, *371*, 144.
(21) Dorfman, L. M.; Taub, I. A.; Buehler, R., E. *J. Phys. Chem.* **1962**, *36*, 3051.
(22) Land, E. J.; Ebert, M. *Trans. Faraday Soc.* **1967**, *63*, 1181.
(23) Neta, P.; Fessenden, R. W. *J. Phys. Chem.* **1974**, *78*, 523.
(24) Micic, O. I.; Nenadovic, M. T. *J. Phys. Chem.* **1976**, *80*, 940.
(25) Sato, K.; Takimoto, K.; Tsuda, S. *Environ. Sci. Technol.* **1978**, *12*, 1043.
(26) Hashimoto, S.; Miyata, T.; Washino, M.; Kawakami, W. *Environ. Sci. Technol.* **1979**, *13*, 71.
(27) Raghavan, N. V.; Steenken, S. *J. Am. Chem. Soc.* **1980**, *102*, 3495.
(28) Bottura, G.; Bubani, B.; Barker, G. C. *J. Electroanal. Chem.* **1981**, *119*, 331.
(29) Field, R. J.; Raghavan, N. V.; Brummer, J. G. *J. Phys. Chem.* **1982**, *86*, 2443.
(30) Matthews, R. W.; McEvoy, S. R. *J. Photochem. Photobiol. A* **1992**, *64*, 231.
(31) Goldstein, S.; Czapski, G.; Rabani, J. *J. Phys. Chem.* **1994**, *98*, 6586.
(32) Ashton, L.; Buxton, G. V.; Stuart, C. R. *J. Chem. Soc., Faraday Trans.* **1995**, *91*, 1631.
(33) Getoff, N. *Rad. Phys. Chem.* **1996**, *47*, 581.
(34) Mvula, E.; Schuchmann, M. N.; von Sonntag, C. *J. Chem. Soc., Perkin Trans. 2* **2001**, *3*, 264.
(35) Olariua, R. I.; Klotzc, B.; Barnesa, I.; Beckera, K. H.; Mocanu, R. *Atmos. Environ.* **2002**, *36*, 3685−3697.
(36) Berndt, T.; Böge, O. *Phys. Chem. Chem. Phys.* **2003**, *5*, 342.
(37) Mvula, E.; Von Sonntag, C. *Org. Biomol. Chem.* **2003**, *1*, 1749.
(38) Monod, A.; Poulain, L.; Grubert, S.; Voisin, D.; Wortham, H. *Atmos. Environ.* **2005**, *39*, 7667−7688.
(39) Lundqvist, M. J.; Eriksson, L. A. *J. Phys. Chem. B* **2000**, *104*, 848.
(40) Steenken, S. *J. Chem. Soc., Faraday Trans. 1* **1987**, *83*, 113.
(41) Roder, M.; Wojnárovits, L.; Földiák, G.; Emmi, S. S.; Beggiato, G.; D'Angelantonio, M. *Rad. Phys. Chem.* **1999**, *54*, 475.
(42) Chen, X.; Schuler, R. H. *J. Phys. Chem.* **1993**, *97*, 421.
(43) Bansal, K. M.; Henglein, A. *J. Phys. Chem.* **1974**, *78*, 160.
(44) Peräkylä, M.; Pakkanen, T. A. *J. Chem. Soc., Perkin Trans. 2* **1995**, *1995*, 1405.
(45) Janata, E.; Schuler, R. H. *J. Phys. Chem.* **1982**, *86*, 2078.
(46) Klein, G. W.; Schuler, R. H. *Int. J. Radiat. Phys. Chem.* **1978**, *11*, 167.
(47) Janik, I.; Marin, T.; Jonah, C. D.; Bartels, D. M. *J. Phys. Chem. A* **2007**, *111*, 79−88.
(48) Herrmann, H. *Chem. Rev.* **2003**, *103*, 4691.
(49) Asmus, K. D.; Cercek, B.; Ebert, M.; Henglein, A.; Wigger, A. *Trans. Faraday Soc.* **1967**, *63*, 2435.
(50) Wander, R.; Neta, P.; Dorfman, L. M. *J. Phys. Chem.* **1968**, *72*, 2946.
(51) Buxton, G. V.; Langan, J. R.; Smith, J. R. L. *J. Phys. Chem.* **1986**, *90*, 6309.
(52) Gordon, S.; Schmidt, K. H.; Hart, E. J. *J. Phys. Chem.* **1977**, *81*, 104.
(53) Bjergbakke, E.; Sillesen, A.; Pagsberg, P. *J. Phys. Chem.* **1996**, *100*, 5729.
(54) Perry, R. A.; Atkinson, R.; Pitts, J. N. J. *J. Phys. Chem.* **1977**, *81*, 296.
(55) Tully, F. P.; Ravishankara, A. R.; Thompson, R. L.; Nicovlch, J. M.; Shah, R. C.; Kreutter, N. M.; Wine, P. H. *J. Phys. Chem.* **1981**, *85*, 2262.
(56) Knispel, R.; Roch, R.; Siese, M.; Zetzsch, C. *Ber. Bunsen-Ges.* **1990**, *94*, 1375.
(57) Lay, T. H.; Bozzelli, J. W.; Seinfeld, J. H. *J. Phys. Chem.* **1996**, *100*, 6543.
(58) Witte, F. U., E.; Zetzsch, C. *J. Phys. Chem.* **1986**, *90*, 3251.
(59) Eberhardt, M. K. *J. Am. Chem. Soc.* **1981**, *103*, 3876.
(60) Elliot, J. A.; Chenier, M. P.; Ouellette, D. C. *J. Chem. Soc., Faraday Trans.* **1993**, *89*, 1193.
(61) Janik, D.; Janik, I.; Bartels, D. M. *Radiat. Res.*, manuscript in preparation.
(62) Lin, M.; Katsumura, Y.; He, H.; Muroya, Y.; Han, Z.; Miyazaki, T.; Kudo, H. *J. Phys. Chem. A* **2005**, *109*, 2847.
(63) Schuler, R. H.; Buzzard, G. K. *Int. J. Radiat. Phys. Chem.* **1976**, *8*, 563.
(64) Ye, M.; Madden, K. P.; Fessenden, R. W.; Schuler, R. H. *J. Phys. Chem.* **1986**, *90*, 5397.
(65) Stalin, T.; Anitha Devi, R.; Rajendiran, N. *Spectrochim. Acta A* **2005**, *61*, 2495.
(66) Ye, M.; Schuler, R. H. *J. Phys. Chem.* **1989**, *93*, 1898.

(67) Jin, F.; Leitich, J.; Von Sonntag, C. *J. Chem. Soc., Perkin Trans. 2* **1993**, *9*, 1583.

(68) Asmus, K. D.; Moeckel, H.; Henglein, A. *J. Phys. Chem.* **1973**, *77*, 1213.

(69) Tripathi, G. N. R.; Su, Y. *J. Phys. Chem. A* **2004**, *108*, 3478.

(70) Hill, P. G. *J. Phys. Chem. Ref. Data* **1990**, *19*, 1233.

(71) Pan, X.-Y.; Schuchmann, M. N.; von Sonntag, C. *J. Chem. Soc., Perkin Trans. 2* **1993**, *3*, 289.

(72) Adams, G. E.; Boag, J. W.; Michael, B. D. *Trans. Faraday Soc.* **1965**, *61*, 1417.

(73) Chen, C.-C.; Bozzelli, J. W.; Farell, J. T. *J. Phys. Chem. A* **2004**, *108*, 4632.

(74) Ghandi, K.; Addison-Jones, B.; Brodovitch, J. C.; McKenzie, I.; Percival, P. W.; Schüth, J. *Phys. Chem. Chem. Phys.* **2002**, *29*, 586.

(75) Roduner, E.; Bartels, D. M. *Ber. Bunsen-Ges.* **1992**, *96*, 1037.